Letter | Editors' Suggestion

# Coexistence of trihexagonal and star-of-David pattern in the charge density wave of the kagome superconductor $AV_3Sb_5$

Yong Hu (胡勇),[1,*] Xianxin Wu (吴贤新),[2,3,†] Brenden R. Ortiz,[4] Xinloong Han (韩欣龙),[5] Nicholas C. Plumb,[1] Stephen D. Wilson,[4] Andreas P. Schnyder,[2] and Ming Shi (史明)[1,‡]

[1]*Photon Science Division, Paul Scherrer Institute, CH-5232 Villigen PSI, Switzerland*

[2]*CAS Key Laboratory of Theoretical Physics, Institute of Theoretical Physics, Chinese Academy of Sciences, Beijing 100190, China*

[3]*Max-Planck-Institut für Festkörperforschung, Heisenbergstrasse 1, D-70569 Stuttgart, Germany*

[4]*Materials Department, University of California Santa Barbara, Santa Barbara, California 93106, USA*

[5]*Kavli Institute of Theoretical Sciences, University of Chinese Academy of Sciences, Beijing 100049, China*

(Received 2 February 2022; revised 29 August 2022; accepted 18 November 2022; published 16 December 2022)

The recently discovered layered kagome metals $AV_3Sb_5$ ($A$ = K, Rb, Cs) have attracted much attention because of their unique combination of superconductivity, charge density wave (CDW) order, and nontrivial band topology. The CDW order with an in-plane 2×2 reconstruction is found to exhibit exotic properties, such as time-reversal symmetry breaking and rotational symmetry breaking. However, the nature of the CDW, including its dimensionality, structural pattern, and effect on electronic structure, remains elusive despite intense research efforts. Here, we present a comprehensive study on the electronic structure of $AV_3Sb_5$ by combining polarization- and temperature-dependent angle-resolved photoemission spectroscopy with density-functional theory calculations. Apart from the energy shift of van Hove singularities, we observe double-band splittings for V $d$-orbital bands in the CDW phase, which provide essential information for revealing the dimensionality and pattern of the CDW order. Our calculations show that three-dimensional CDW orders containing stacking of star-of-David and trihexagonal patterns along the $c$ axis can quantitatively reproduce the experimental features. The characteristic splittings from the two patterns can be experimentally extracted and they are quantitatively consistent with calculations, clearly demonstrating intrinsic coexistence of the two patterns in the CDW order. These results provide crucial insights into the nature and distortion pattern of the CDW order, and its signature in the electronic structure, thereby laying down the basis for a substantiated understanding of the exotic properties in the family of $AV_3Sb_5$ kagome metals.

DOI: 10.1103/PhysRevB.106.L241106

Transition-metal based kagome materials, owing to the unique lattice geometry, provide a fascinating platform to study spin liquid states [1–6], flat bands [7], superconductivity [8–11], charge density wave (CDW) order [9–13], and topological physics [14–17]. Recently, the discovery of a new class of kagome metals $AV_3Sb_5$ ($A$ = K, Rb, Cs), exhibiting topologically nontrivial electronic structure, unconventional superconductivity, and CDW order, have been attracting tremendous attention [18–51]. Superconductivity emerges inside the CDW order with a critical temperature $T_C \sim$ 0.9–2.5 K at ambient pressure [19–21], showing double-superconducting domes under pressure [28–30]. The CDW phase transition occurs at $T_{CDW} \sim$ 78–103 K [19,21,32], for which scanning tunneling microscopy (STM) suggested a 2×2 in-plane reconstruction [32–34]. In addition, an enhanced relaxation rate in the CDW phase from recent zero-field $\mu$SR experiments is in line with a broken time-reversal symmetry [35,36], which could be intimately related to the observed giant anomalous Hall effect [37,38]. Furthermore, CDW order possessing lattice rotational symmetry breaking [39] can be inferred owing to the twofold symmetrical $c$-axis resistivity from magnetoresistance measurements [40]. Theoretical studies provide two scenarios about the in-plane CDW order: phonon softening [41,42] and interaction-driven Fermi surface instability, i.e., a loop current order [43–46].

Despite intensive studies on the CDW, its nature still remains elusive. Modulation along the $c$ direction further revealed by x-ray diffraction (XRD) and STM experiments implies a three-dimensional (3D) CDW order [32,47]. In spite of a 2×2×2 modulation from STM measurements [48], XRD measurements suggest a 2×2×4 reconstruction [49]. Very recently a transition between these two phases was found through varying temperature [50]. Moreover, the CDW structural pattern in the kagome layers is still unclear: NMR measurements tend to suggest a star of David (SoD) distortion [51], although the trihexagonal (TrH) distortion is theoretically more stable [41,42]. So far, the structural pattern could not be pinned down from STM and XRD measurements. Despite the experimental evidence for the 3D nature of the CDW order, direct evidence for its effect on the vanadium $d$-orbital band dispersions associated with the kagome lattice in $AV_3Sb_5$ is still lacking, which would be very helpful in revealing the spectroscopic fingerprints of the CDW pattern. A

*yonghphysics@gmail.com
†xianxin.wu@fkf.mpg.de
‡ming.shi@psi.ch

 

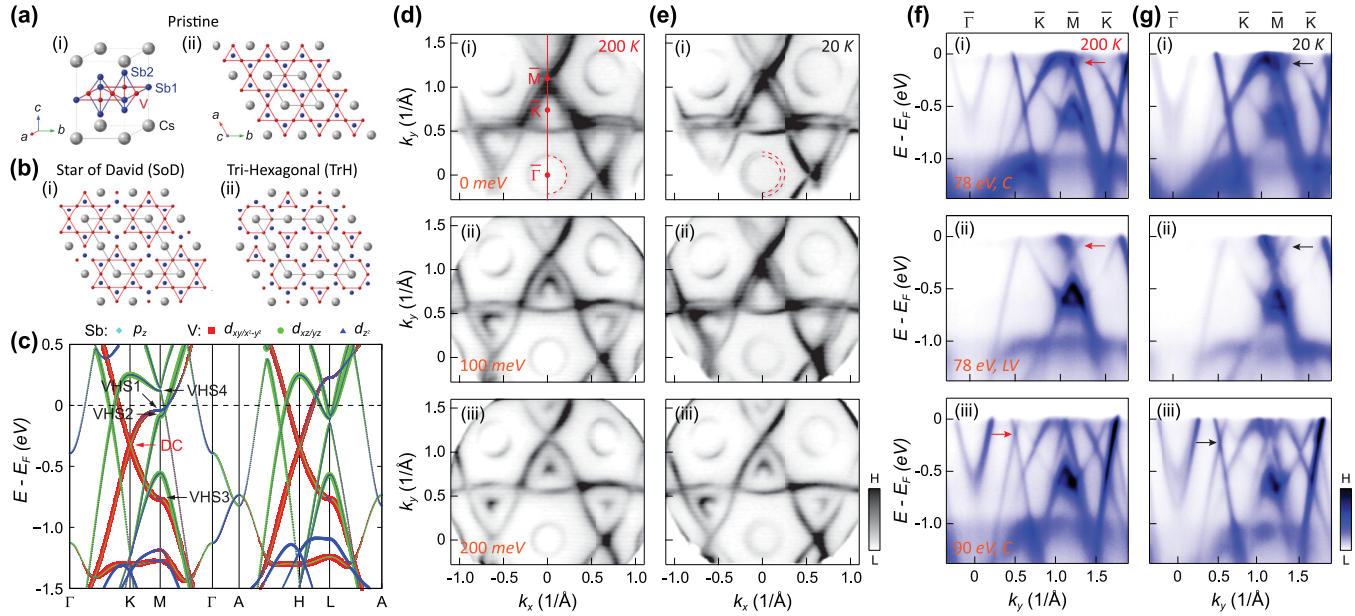


FIG. 1. Crystal and electronic structures of $CsV_3Sb_5$ above and below $T_{CDW}$. (a), (b) Crystal structure in the normal state (a), and CDW phase (b) with the candidate SoD structure (i) and TrH structure (ii). (c) DFT calculations for the orbital character resolved band structure. (d), (e) CECs at different binding energies, measured at 200 (d) and 20 K (e). (f), (g) ARPES spectra obtained at 200 (f) and at 20 K (g).

detailed understanding of the 3D CDW structural pattern, and in particular the ensuing electronic structure reconstruction, are of crucial importance for understanding the nature and origin of the CDW order and its interplay with superconductivity.

In this work, we used polarization- and temperature-dependent angle-resolved photoemission spectroscopy (ARPES) to reveal the nature of the CDW in the kagome superconductors $AV_3Sb_5$ from an electronic perspective. Upon cooling, the energy location of the two near-$E_F$ VHSs is found to suddenly drop by about 90 meV, once the temperature falls below $T_{CDW}$. Moreover, universal band-splitting-like features on the kagome bands are revealed, exhibiting prominent band-folding effects in the kagome lattice, which can be well captured by the density-functional theory (DFT) calculations including superimposed trihexagonal and star-of-David CDW patterns. The characteristic splittings from the two patterns are experimentally extracted (Table I in the Supplemental Material [52]; see also Refs. [22,24,41,53–62] therein), and they are almost quantitatively consistent with calculations, clearly demonstrating intrinsic coexistence of two patterns in the CDW order. These findings not only provide essential insights into the band reconstructions of the CDW order but also unambiguously identify the 3D nature and CDW distortion pattern, which will be crucial in illuminating its mechanism.

The pristine phase of $CsV_3Sb_5$ crystallizes in a layered crystal structure with the space group $P6/mmm$ (No. 191) [Fig. 1(a)]. It consists of $V_3Sb$ kagome layers bounded above and below by Sb honeycomb layers and Cs hexagonal networks [Fig. 1(a)(i)]. Below the CDW transition temperature ($T_{CDW} = 94$ K), the kagome layer can exhibit two types of distortions derived from breathing phonon modes [41]: a star of David [Fig. 1(b)(i)] and its inverse structure (trihexagonal) [Fig. 1(b)(ii)]. The orbital-resolved band structure of pristine $CsV_3Sb_5$ from DFT calculations is shown in Fig. 1(c), where Sb-$p_z$ orbital contributes an electron band around the Brillouin-zone center and vanadium $d$ orbitals dominate the Dirac cone (DC) bands around the $K$ point and four-fold van Hove singularity (VHS) bands around the $M$ point with diverse sublattice features. To demonstrate the effect of CDW order on the electronic structure, we first compare the ARPES spectra of $CsV_3Sb_5$ in the normal state ($T \gg T_{CDW}$) and CDW phase ($T \ll T_{CDW}$). Figure 1(d) plots the constant energy contours (CECs) and their evolution with binding energy ($E_B$) measured at 200 K. With increasing $E_B$, the Sb contributed circular-shaped pocket near the zone center ($\bar{\Gamma}$ point) and triangle-shaped Fermi surface derived from the vanadium kagome lattice around the $\bar{K}$ points shrink [Figs. 1(d)(i)–(iii)], reflecting their electron-like nature. In the CDW states, one prominent change is that the electron pocket around $\bar{\Gamma}$ is doubled [Figs. 1(e)(i)–(iii)], which has been suggested to originate from the $k_z$ broadening [63], quantum-well states on the surface [64], or the out-of-plane band folding [53]. Moreover, the triangle-shaped CECs associated with the vanadium $d$ orbitals around $\bar{K}$ enlarge slightly in the CDW phase [Figs. 1(e)(i)–(iii)], compared with the corresponding CECs at the same $E_B$ in the normal state [Figs. 1(d)(i)–(iii)]. To further identify the effect of CDW order, we compare the band dispersions along the $\bar{\Gamma}$-$\bar{K}$ direction above and below the $T_{CDW}$. ARPES spectra reveal a downward shift of the bands around $\bar{M}$ point in the CDW phase [Figs. 1(f)(i) and 1(g)(i)], which is more evident with linear vertically ($LV$) polarized light [see the arrows in Figs. 1(f)(ii) and 1(g)(ii)]. The Dirac-like crossing point between the $\bar{\Gamma}$ and $\bar{K}$ points also shifts down significantly in energy in the CDW state, as indicated by the arrow in Figs. 1(f)(iii) and 1(g)(iii) (for details, see Fig. S1). Since

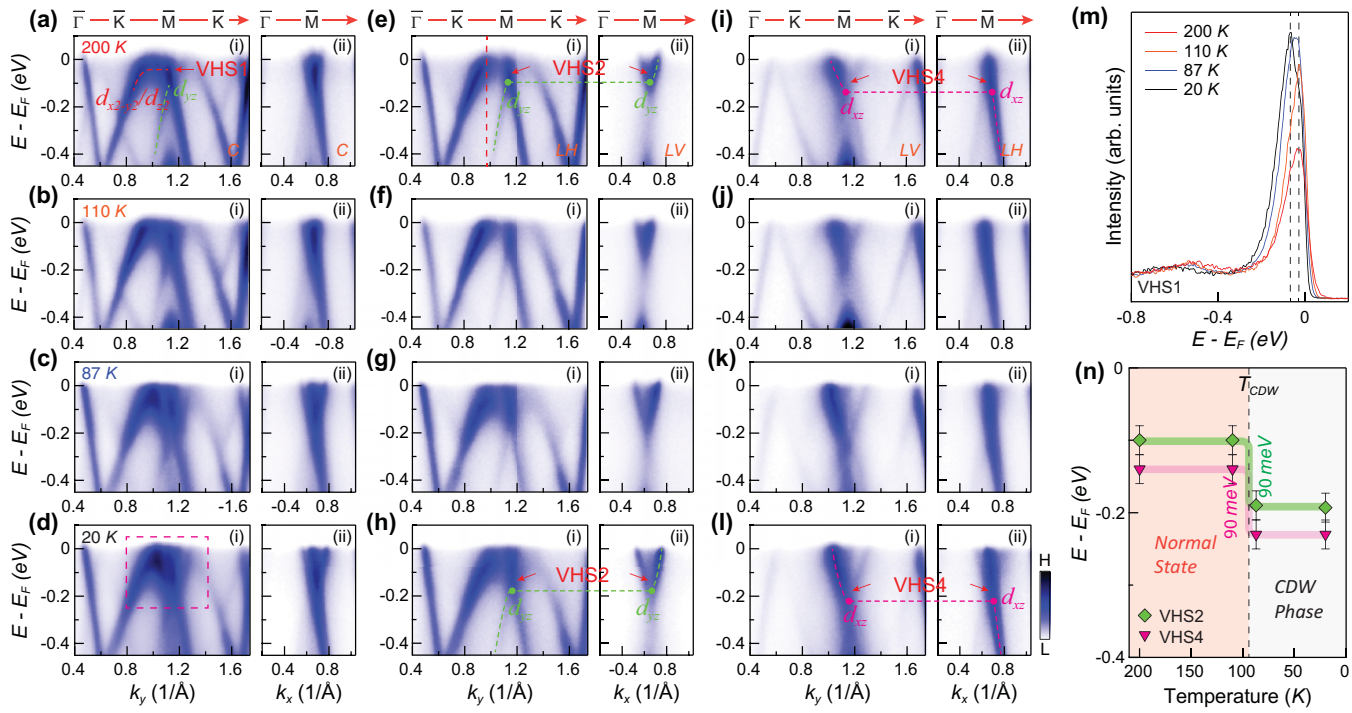


FIG. 2. Temperature and polarization dependence of the electronic structure. (a)–(d) ARPES spectra taken along the $\bar{\Gamma}$-$\bar{K}$ [(i)] and $\bar{\Gamma}$-$\bar{M}$ [(ii)] directions, measured at 200 (a), 110 (b), 87 (c), and 20 K (d) with 78-eV *C* polarized light. (e)–(h), (i)–(l) Same as (a)–(d), but obtained with *LH* [(e)–h(i), (i)–l(ii)] and *LV* [(e)–h(ii), (i)–l(i)] polarizations. Dashed curves are guide to the eye for the kagome bands around the $\bar{M}$ point. Red arrow indicates VHSs. (m) Temperature evolution of the EDCs taken around the flat feature of VHS1. Position of the EDCs is indicated by the red dashed line in [e(i)]. (n) Energy location of VHS2 and VHS4 as a function of temperature. The VHS positions are determined by the band bottom and top position at the *M* point.

there are multiple VHSs located around the $\bar{M}$ point [Fig. 1(c) [24], carrying large density of states, the CDW-induced band reconstruction on them could be prominent.

To further demonstrate the salient features of the band reconstruction at the VHSs in the CDW phase, we performed systematic temperature-dependent measurements on $CsV_3Sb_5$ (Fig. 2). Upon cooling, the overall evolution of the band structures can be divided into two distinct regions: above and below the $T_{CDW}$. As shown in Fig. 2(a), above $T_{CDW}$, the band dispersion remains almost unchanged [Figs. 2(a) and 2(b)], while once below $T_{CDW}$, the pronounced band reconstruction around $\bar{M}$ can be observed [Figs. 2(c) and 2(d)], as highlighted by the pink box in Fig. 2(d)(i)]. To clearly disentangle the bands and keep track of the energy location of the VHSs, we show the polarization dependence of the spectra in Figs. 2(e)–2(l). Cooling from the normal state to the CDW phase, VHS1 band exhibits unusual spectral broadening along the $\bar{K}$-$\bar{M}$ direction in the CDW phase [Figs. 2(e)–2(f)(i)], as evidenced by the temperature-dependent energy distribution curves (EDCs) taken near the flat feature of VHS1 [Fig. 2(m)]. Under our ARPES geometry (for details, see Fig. S2), VHS2 bands ($d_{yz}$ orbital) along the $\bar{\Gamma}$-$\bar{K}$ [Figs. 2(e)–2(h)(i)] and $\bar{\Gamma}$-$\bar{M}$ [Figs. 2(e)–2(h)(ii)] directions are detected by linear horizontally (*LH*) and *LV* polarized light, respectively [24], while the VHS4 bands [23] with $d_{xz}$ character along the $\bar{\Gamma}$-$\bar{K}$ [Figs. 2(i)–2(l)(i)] and $\bar{\Gamma}$-$\bar{M}$ [Figs. 2(i)–2(l)(ii)] paths are favored under the *LV* and *LH* polarizations, respectively. The energy location of VHS2 (respectively, VHS4) is determined by the $d_{xz}$ bottom and top (respectively, $d_{yz}$-band bottom) along the $\bar{\Gamma}$-$\bar{K}$ and its band bottom (respectively, band top) along the $\bar{\Gamma}$-$\bar{M}$ direction. Figure 2(n) shows the temperature dependence of the energy locations of VHS and VHS4, which suddenly drop in energy across the CDW transition by about 90 meV. The band shifts take place suddenly when the system enters the CDW phase (Fig. 2), suggesting that they are intimately related to the CDW order and the CDW transition is first order.

Besides the energy shift of the VHSs, we further display the characteristic double-band splitting features on the vanadium *d* orbitals of the CDW phase in detail along high-symmetry paths [Figs. 3(a)–3(f)]. In Figs. 3(a) and 3(b), we show the temperature dependence of the ARPES spectra collected under circular (*C*) polarization along the $\bar{\Gamma}$-$\bar{K}$ direction. Remarkably, compared to the bands measured above $T_{CDW}$, the spectra taken below $T_{CDW}$ exhibit diverse band-splitting-like features on the *d*-orbital bands in almost the entire energy-momentum space [indicated by the red dashed line and arrow in Fig. 3(b)(i)]. Specifically, splittings occur near the Fermi level (BS1), on the lower branch of the Dirac cone band along the $\bar{\Gamma}$-$\bar{M}$ direction (marked as BS2, B3), around the VHS3 bands (BS4), and even on the bands with an $E_B$ lower than 1.0 eV (BS5, BS6). Consistently, the double-band splittings can also be clearly seen in the bands measured at low temperature [Figs. 3(d) and 3(e)], along the $\bar{\Gamma}$-$\bar{M}$ direction [marked as BS7-BS9 in Fig. 3(e)(i); for details, see Fig. S3]. By showing the ARPES spectra below

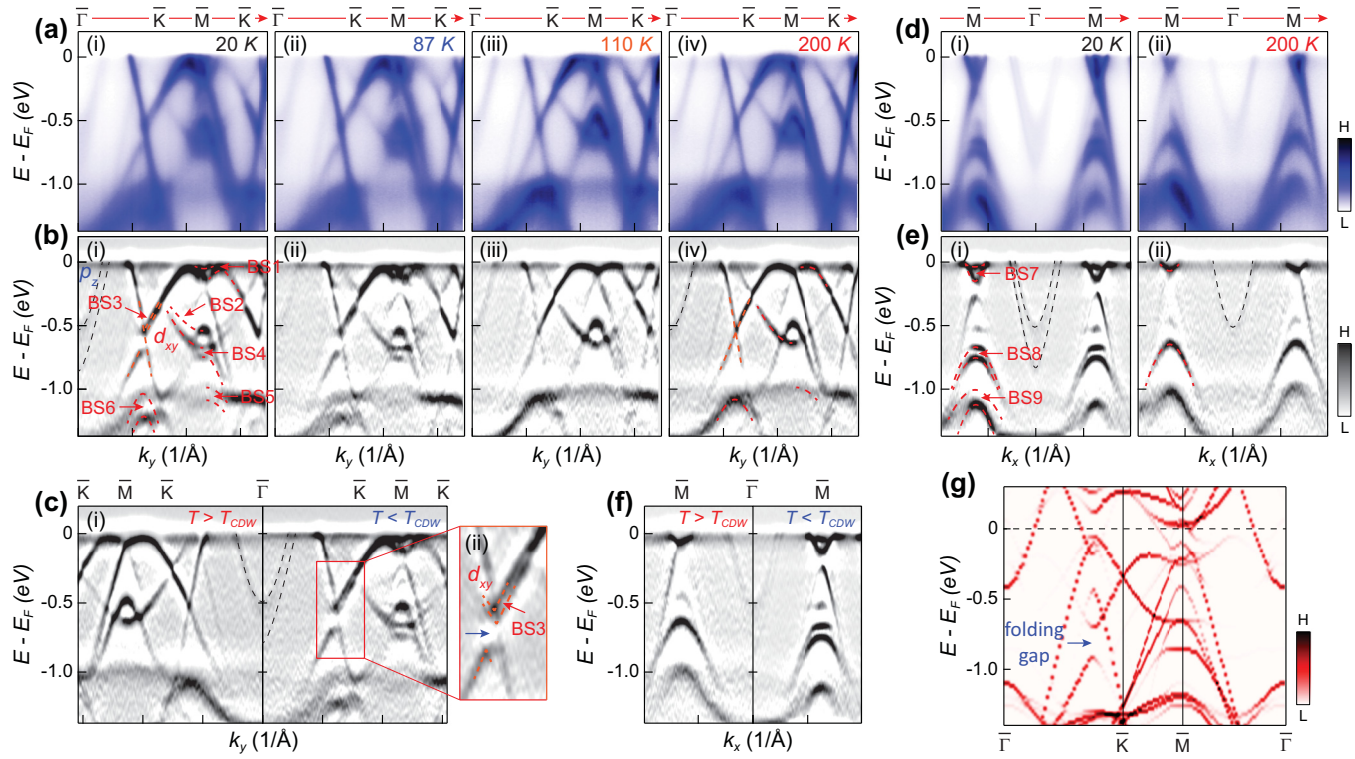


FIG. 3. Double-band splitting features of kagome bands below $T_{CDW}$.(a), (b) ARPES spectra (a) and their curvature plots (b) at different temperatures, taken along the $\bar{\Gamma}$-$\bar{K}$ direction. (c) Comparison of the curvature plots taken at 200 and 20 K. The orange box in (i) highlights the folding gap (ii). (d)–(f) Same as (a)–(c), but measured along the $\bar{\Gamma}$-$\bar{M}$ direction. Red arrows indicate the double-band splittings in the CDW phase. (g) DFT calculations for the band structures of 2×2 TrH phase.

and above $T_{CDW}$ in the same plot, Figs. 3(c) and 3(f) highlight the marked contrast between the bands in the normal state and CDW phase. Besides the double-band splitting features, CDW folding gaps of the $d_{xy}$ band can be identified along the $\bar{\Gamma}$-$\bar{K}$ direction [indicated by the blue arrow in Fig. 3(c)(ii)], which is consistent with the observation in $KV_3Sb_5$ [25]. Moreover, we have checked the band structure of $RbV_3Sb_5$ in the CDW phase, and found a similar band reconstruction (see Fig. S4 for details). Therefore, these results [Figs. 3(a)–3(e)] and Fig. S4) strongly demonstrate that the observed double-band splitting features are directly derived from the CDW order. However, these features cannot be explained by an in-plane CDW order. As shown Fig. 3(g), we show the unfolded band structure of $CsV_3Sb_5$ by considering the 2×2 TrH reconstruction [Fig. 1(b)(ii)]. While the two-dimensional (2D) lattice reconstruction can only qualitatively capture the folding gap along the $\bar{\Gamma}$-$\bar{K}$ direction [see the blue arrow in Figs. 3(c)(ii) and 3(g)], the new emergent bands observed in the CDW phase are completely missing.

Motivated by the suggested 2×2×2 CDW order from recent XRD and STM measurements in $AV_3Sb_5$, we further explore the band reconstructions from a 3D CDW order. For the 2×2×2 CDW order, consisting of SoD- or TrH-like distortions, there are four possible configurations along the $c$ axis: SoD-$\pi$, TrH-$\pi$, SoD-TrH-$\pi$, and SoD-TrH, where $\pi$ denotes an in-plane $\pi$-phase shift between adjacent kagome layers (see Fig. S5 for details). The unfolded band dispersions for the SoD-$\pi$ and TrH-$\pi$ configurations are displayed in Figs. 4(a) and 4(b), respectively (see Figs. S6 and S7 for the dispersions along other paths). In the SoD-$\pi$ configuration, the VHS1, VHS2, and VHS4 bands around the $\bar{M}$ point are gapped [indicated by the green arrow in Fig. 4(a)]. In addition, two folding gaps for the $d_{xy}$ band along the $\bar{\Gamma}$-$\bar{K}$ direction above and below the band crossing can be clearly identified (marked as black arrow). The band reconstruction in the TrH-$\pi$ configuration is similar but with much larger splitting and gap, especially for the VHS1 and VHS2 bands. However, these band reconstructions are similar to those from 2D SoD or TrH distortions except for some noticeable band folding around $\bar{\Gamma}$, and thus cannot explain the doubled-splitting features in experiments. We further display the unfolded band dispersion for the structures with alternating SoD- and TrH-like distortions in Figs. 4(c) (SoD-TrH-$\pi$) and 4d (SoD-TrH). The band dispersion in both cases is relatively similar and the band reconstruction consists of contributions from both SoD- and TrH-like distortions, generating double-splitting features. Interestingly, the splitting of the lower Dirac cone bands along the $\bar{K}$-$\bar{M}$ can be clearly identified [marked as BS2 in Figs. 4(d) and 4(e)]. By comparing Fig. 4(e) and Figs. 4(c) and 4(d), we find that the observed band reconstructions (BS1, BS2, BS4, BS5, BS7-BS9) in ARPES experiments can be well reproduced from these two distortions. As the SoD- and TrH-like distortions exhibit distinct splittings and folding gaps, we can further extract the energy scales of the splitting $\Delta_1$ around the $\bar{M}$ point, the CDW folding gap $\Delta_2$ along the $\bar{K}$-$\bar{M}$ direction, the flat $d_{xy}/d_{x^2-y^2}$-band splitting $\Delta_3$, and the near-$E_F$-band

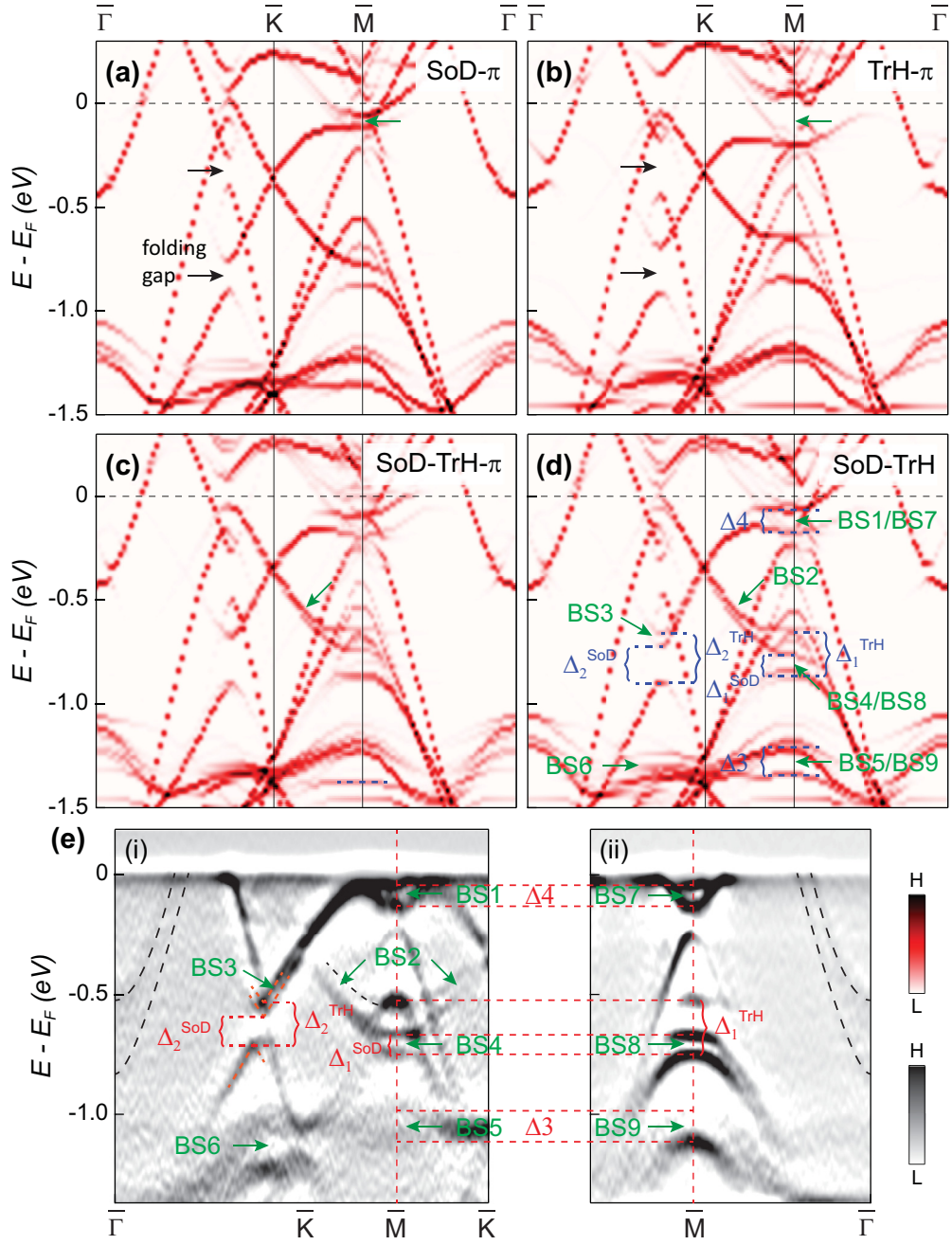


FIG. 4. Unfolded band structures in 2×2×2 CDW order from calculations. (a)–(d) Band structures of the following lattice configurations: SoD-$\pi$ (a), TrH-$\pi$ (b), SoD-TrH-$\pi$ (c), and SoD-TrH (d). Blue dashed lines define the splitting gaps ($\Delta_1$, $\Delta_3$, $\Delta_4$,) and folding gaps ($\Delta_2$). Superscripts SoD and TrH in the gaps ($\Delta_1$, $\Delta_2$) represent the contributions of the two configurations, respectively. (e) ARPES spectra taken at 20 K along the $\bar{\Gamma}$-$\bar{K}$ (i) and $\bar{\Gamma}$-$\bar{M}$ (ii) directions.

splitting $\Delta_4$, for $CsV_3Sb_5$ in experiments. We summarize the experimental values in Fig. S8, in comparison to theoretical values. It is striking that the experimental values are in good agreement with the theoretical values of the SoD-TrH-$\pi$ and SoD-TrH configurations. The in-plane SoD and TrH domains might generate similar band splittings but they have a significant energy cost [41], which is unlikely to occur in realistic materials [65] (see details in Sec. 9 in Ref. [52]).

Our ARPES measurements, combined with DFT calculations, unambiguously reveal band reconstructions originating from both SoD- and TrH-like distortions. This demonstrates the coexistence of the two distortions in the CDW phase, although the SoD phase is theoretically believed to be metastable. These distortions lead to strong reconstructions of both the VHS bands and the vanadium $d$-orbital bands. The stacking of the two distortions along the $c$ axis can generate a 3D CDW order. Their alternating stacking yields a 2×2×2 CDW order. More complicated stacking, such as $TS\bar{T}\bar{S}$ and TTST, where $\bar{T}$ or $\bar{S}$ denotes an in-plane $\pi$ shift, can quadruple the unit cell along the $c$ axis and lead to

a 2×2×4 CDW order (see Fig. S9 for the calculations of TS$\bar{\text{T}}\bar{\text{S}}$ stacking), which is suggested by recent XRD measurements [49,50]. In the CDW phase, the experimental transition between 2×2×2 and 2×2×4 reconstructions by varying temperature could be related to the change of distortion stacking along the $c$ axis [50]. One important feature of a 3D CDW order is that the sixfold rotational symmetry can be broken for the distortions involving an in-plane $\pi$ shift between adjacent layers. The SoD-TrH-$\pi$ configuration can account for the observed twofold symmetrical $c$-axis resistivity in experiments [40]. In addition, although the observed splitting of the Sb $p_z$-orbital bands near Γ are missing in our calculations (possibly due to correlation effects or an underestimation of the Sb distortion), the band folding along the $c$ axis due to the 3D nature of the CDW order provides a qualitatively better account of the ARPES data. While the DFT calculations based on static lattice distortions go a long way in reproducing our band-structure measurements in the CDW phase, they do not account for the time-reversal symmetry breaking seen in other experiments [32,35]. This suggests that electron-phonon coupling [25,66] and electron-electron interactions may conspire to generate the unconventional CDW order in $AV_3Sb_5$ kagome metals, which deserves further investigations, both from the theoretical and the experimental side.

Y.H. was supported by the National Natural Science Foundation of China (Grant No. 12004363). The work at PSI was supported by the Swiss National Science Foundation under Grant. No. 200021_188413, and the Sino-Swiss Science and Technology Cooperation (Grant No. IZLCZ2_170075). The work at UC Santa Barbara was supported via the UC Santa Barbara NSF Quantum Foundry funded via the Q-AMAIE-i program under Award No. DMR-1906325. This research made use of the shared facilities of the NSF Materials Research Science and Engineering Center at UC Santa Barbara (Grant No. DMR-1720256). B.R.O. acknowledges support from the California NanoSystems Institute through the Elings Fellowship program.

[1] M. R. Norman, Colloquium: Herbertsmithite and the search for the quantum spin liquid, Rev. Mod. Phys. **88**, 041002 (2016).
[2] D. Wulferding, P. Lemmens, P. Scheib, J. Roder, P. Mendels, S. Chu, T. Han, and Y. S. Lee, Interplay of thermal and quantum spin fluctuations in the kagome lattice compound herbertsmithite, Phys. Rev. B **82**, 144412 (2010).
[3] S. Yan, D. A. Huse, and S. R. White, Spin-liquid ground state of the S½1/2 Kagome Heisenberg antiferromagnet, Science **332**, 1173 (2011).
[4] T.-H. Han, J. S. Helton, S. Chu, D. G. Nocera, J. A. Rodriguez-Rivera, C. Broholm, and Y. S. Lee, Fractionalized excitations in the spin-liquid state of a kagome-lattice antiferromagnet, Nature (London) **492**, 406 (2012).
[5] T. Han, S. Chu, and Y. S. Lee, Refining the Spin Hamiltonian in the Spin-1/2 Kagome Lattice Antiferromagnet $ZnCu_3(OH)_6Cl_2$ Using Single Crystals, Phys. Rev. Lett. **108**, 157202 (2012).
[6] M. Fu, T. Imai, T.-H. Han, and Y. S. Lee, Evidence for a gapped spin-liquid ground state in a kagome Heisenberg antiferromagnet, Science **350**, 655 (2015).
[7] J.-X. Yin, S. S. Zhang, G. Chang, Q. Wang, S. S. Tsirkin, Z. Guguchia, B. Lian, H. Zhou, K. Jiang, I. Belopolski, N. Shumiya, D. Multer, M. Litskevich, T. A. Cochran, H. Lin, Z. Wang, T. Neupert, S. Jia, H. Lei, and M. Z. Hasan, Negative flat band magnetism in a spin–orbit- coupled correlated kagome magnet, Nat. Phys. **15**, 443 (2019).
[8] W.-H. Ko, P. A. Lee, and X.-G. Wen, Doped kagome system as exotic superconductor, Phys. Rev. B **79**, 214502 (2009).
[9] M. L. Kiesel and R. Thomale, Sublattice interference in the kagome Hubbard model, Phys. Rev. B **86**, 121105(R) (2012).
[10] M. L. Kiesel, C. Platt, and R. Thomale, Unconventional Fermi Surface Instabilities in the Kagome Hubbard Model, Phys. Rev. Lett. **110**, 126405 (2013).
[11] W.-S. Wang, Z.-Z. Li, Y.-Y. Xiang, and Q.-H. Wang, Competing electronic orders on kagome lattices at van Hove filling, Phys. Rev. B **87**, 115135 (2013).
[12] H.-M. Guo and M. Franz, Topological insulator on the kagome lattice, Phys. Rev. B **80**, 113102 (2009).
[13] S. Isakov, S. Wessel, R. Melko, K. Sengupta, and Y. B. Kim, Hard-Core Bosons on the Kagome Lattice: Valence-Bond Solids and Their Quantum Melting, Phys. Rev. Lett. **97**, 147202 (2006).
[14] L. Ye, M. Kang, J. Liu, F. Cube, C. R. Wicker, T. Suzuki, C. Jozwiak, A. Bostwick, E. Rotenberg, D. C. Bell, L. Fu, R. comin, and J. G. Checkelsky, Massive Dirac fermions in a ferromagnetic kagome metal, Nature (London) **555**, 638 (2018).
[15] J.-X. Yin, W. Ma, T. A. Cochran, X. Xu, S. S. Zhang, H.-J. Tien, N. Shumiya, G. Cheng, K. Jiang, B. Lian, Z. Song, G. Chang, I. Belopolski, D. Multer, M. Litskevich, Z.-J. Cheng, X. P. Yang, B. Swidler, H. Zhou, H. Lin, T. Neupert, Z. Wang, N. Yao, T.-R. Chang, S. Jia, and M. Z. Hasan, Quantum-limit Chern topological magnetism in $TbMn_6Sn_6$, Nature (London) **583**, 533 (2020).
[16] M. Kang, L. Ye, S. Fang, J.-S. You, A. Levitan, M. Han, J. I. Facio, C. Jozwiak, A. Bostwick, E. Rotenberg, M. K. Chan, R. D. McDonald, D. Graf, K. Kaznatcheev, E. Vescovo, D. C. Bell, E. Kaxiras, J. Brink, M. Richter, M. P. Ghimire, J. G. Checkelsky, and R. Comin, Dirac fermions and flat bands in the ideal kagome metal FeSn, Nat. Mater. **19**, 163 (2020).
[17] H. Tsai, T. Higo, K. Kondou, T. Nomoto, A. Sakai, A. Kobayashi, T. Nakano, K. Yakushiji, R. Arita, S. Miwa *et al.*, Electrical manipulation of a topological antiferromagnetic state, Nature (London) **580**, 608 (2020).
[18] B. R. Ortiz, L. C. Gomes, J. R. Morey, M. Winiarski, M. Bordelon, J. S. Mangum, I. W. Oswald, J. A. Rodriguez-Rivera, J. R. Neilson, and S. D. Wilson, New kagome prototype materials: Discovery of $KV_3Sb_5$, $RbV_3Sb_5$, and $CsV_3Sb_5$, Phys. Rev. Mater. **3**, 094407 (2019).
[19] B. R. Ortiz, S. M. Teicher, Y. Hu, J. L. Zuo, P. M. Sarte, E. C. Schueller, A. M. Abeykoon, M. J. Krogstad, S. Rosenkranz, R. Osborn, R. Seshadri, L. Balents, J. He, and S. D. Wilson, $CsV_3Sb_5$: A $\mathbb{Z}_2$ Topological Kagome Metal with

a Superconducting Ground State, Phys. Rev. Lett. **125**, 247002 (2020).

[20] B. R. Ortiz, P. M. Sarte, E. M. Kenney, M. J. Graf, S. M. L. Teicher, R. Seshadri, and S. D. Wilson, Superconductivity in the $\mathbb{Z}_2$ kagome metal $KV_3Sb_5$, Phys. Rev. Mater. **5**, 034801 (2021).

[21] Q. Yin, Z. Tu, C. Gong, Y. Fu, S. Yan, and H. Lei, Superconductivity and normal-state properties of kagome metal $RbV_3Sb_5$ single crystals, Chin. Phys. Lett. **38**, 037403 (2021).

[22] Y. Hu, S. M. L. Teicher, B. R. Ortiz, Y. Luo, S. Peng, L. Huai, J. Z. Ma, N. C. Plumb, S. D. Wilson, J.-F. He, and M. Shi, Topological surface states and flat bands in the kagome superconductor $CsV_3Sb_5$, Sci. Bull. **67**, 495 (2022).

[23] M. G. Kang, S. Fang, J. Kim, B. R. Ortiz, S. H. Ryu, J. Kim, J. Yoo, G. Sangiovanni, D. D. Sante, B.-G. Park, C. Jozwiak, A. Bostwick, E. Rotenberg, E. Kaxiras, S. D. Wilson, J.-H. Park, and R. Comin, Twofold van Hove singularity and origin of charge order in topological kagome superconductor $CsV_3Sb_5$, arXiv:2105.01689.

[24] Y. Hu, X. Wu, B. R. Ortiz, S. Ju, X. Han, J. Z. Ma, N. C. Plumb, M. Radovic, R. Thomale, S. D. Wilson, A. P. Schnyder, and M. Shi, Rich nature of van Hove singularities in kagome superconductor $CsV_3Sb_5$, Nat. Commun. **13**, 2220 (2022).

[25] H. L. Luo, Q. Gao, H. Liu, Y. Gu, D. Wu, C. Yi, J. Jia, S. Wu, X. Luo, Y. Xu, L. Zhao, Q. Wang, H. Mao, G. Liu, Z. Zhu, Y. Shi, K. Jiang, J. Hu, Z. Xu, and X. J. Zhou, Electronic nature of charge density wave and electron-phonon coupling in kagome superconductor $KV_3Sb_5$, Nat. Commun. **13**, 273 (2022).

[26] L. Nie, K. Sun, W. Ma, D. Song, L. Zheng, Z. Liang, P. Wu, F. Yu, J. Li, M. Shan, D. Zhao, S. Li, B. Kang, Z. Wu, Y. Zhou, K. Liu, Z. Xiang, J. Ying, Z. Wang, T. Wu, and X. Chen, Charge-density-wave-driven electronic nematicity in a kagome superconductor, Nature (London) **604**, 59 (2022).

[27] C. C. Zhao, L. S. Wang, W. Xia, Q. W. Yin, J. M. Ni, Y. Y. Huang, C. P. Tu, Z. C. Tao, Z. J. Tu, C. S. Gong, H. C. Lei, Y. F. Guo, X. F. Yang, and S. Y. Li, Nodal superconductivity and superconducting domes in the topological Kagome metal $CsV_3Sb_5$, arXiv:2102.08356.

[28] K. Y. Chen, N. N. Wang, Q. W. Yin, Z. J. Tu, C. S. Gong, J. P. Sun, H. C. Lei, Y. Uwatoko, and J.-G. Cheng, Double Superconducting Dome and Triple Enhancement of $T_c$ in the Kagome Superconductor $CsV_3Sb_5$ under High Pressure, Phys. Rev. Lett. **126**, 247001 (2021).

[29] Z. Zhang, Z. Chen, Y. Zhou, Y. Yuan, S. Wang, L. Zhang, X. Zhu, Y. Zhou, X. Chen, J. Zhou, and Z. Yang, Pressure-induced reemergence of superconductivity in topological kagome metal $CsV_3Sb_5$, Phys. Rev. B **103**, 224513 (2021).

[30] X. Chen, X. Zhan, X. Wang, J. Deng, X.-B. Liu, X. Chen, J.-G. Guo, and X. Chen, Highly-robust reentrant superconductivity in $CsV_3Sb_5$ under pressure, Chin. Phys. Lett. **38**, 057402 (2021).

[31] Y. Wang, S.-Y. Yang, P. K. Sivakumar, B. R. Ortiz, S. M. L. Teicher, H. Wu, A. K. Srivastava, C. Garg, D. Liu, S. S. P. Parkin, E. S. Toberer, T. McQueen, S. D. Wilson, and M. N. Ali, Proximity-induced spin-triplet superconductivity and edge supercurrent in the topological Kagome metal, $K_{1-x}V_3Sb_5$, arXiv:2012.05898.

[32] Y.-X. Jiang, J.-X. Yin, M. M. Denner, N. Shumiya, B. R. Ortiz, J. He, X.-X. Liu, S.-T. S. Zhang, G.-Q. Chang, I. Belopolski, Q. Zhang, T. A. Cochran, D. Multer, M. Litskevich, Z.-J. Cheng, X. P. Yang, Z. Wang, R. Thomale, T. Neupert, S. D. Wilson, and M. Zahid Hasan, Unconventional chiral charge order in kagome superconductor $KV_3Sb_5$, Nat. Mater. **20**, 1353 (2021).

[33] H. Chen, B. Hu, Z. Zhao, J. Yuan, Y. Xing, G. Qian, Z. Huang, G. Li, Y. Ye, Q. Yin, C. Gong, Z. Tu, H. Lei, S. Ma, H. Zhang, S. Ni, H. Tan, C. Shen, X. Dong, B. Yan, Z. Wang, and H.-J. Gao, Roton pair density wave and unconventional strong-coupling superconductivity in a topological kagome metal, Nature (London) **559**, 222 (2021).

[34] H. Zhao, H. Li, B. R. Ortiz, S. M. L. Teicher, T. Park, M. Ye, Z. Wang, L. Balents, S. D. Wilson, and I. Zeljkovic, Cascade of correlated electron states in a kagome superconductor $CsV_3Sb_5$, Nature (London) **599**, 216 (2021).

[35] C. Mielke, III, D. Das, J.-X. Yin, H. Liu, R. Gupta, C. N. Wang, Y.-X. Jiang, M. Medarde, X. Wu, H. C. Lei, J. J. Chang, P. Dai, Q. Si, H. Miao, R. Thomale, T. Neupert, Y. Shi, R. Khasanov, M. Z. Hasan, H. Luetkens, and Z. Guguchia, Time-reversal symmetry-breaking charge order in a correlated kagome superconductor, Nature (London) **602**, 245 (2022).

[36] L. Yu, C. Wang, Y. Zhang, M. Sander, S. Ni, Z. Lu, S. Ma, Z. Wang, Zhen Zhao, H. Chen, K. Jiang, Y. Zhang, H. Yang, F. Zhou, X. Dong, S. L. Johnson, M. J. Graf, J. Hu, H.-J. Gao, and Z. Zhao, Evidence of a hidden flux phase in the topological kagome metal $CsV_3Sb_5$, arXiv:2107.10714.

[37] S.-Y. Yang, Y. Wang, B. R. Ortiz, D. Liu, J. Gayles, E. Derunova, R. Gonzalez-Hernandez, L. Sˇmejkal, Y. Chen, S. S. P. Parkin, S. D. Wilson, E. S. To- berer, T. McQueen, and M. N. Ali, Giant, unconventional anomalous Hall effect in the metallic frustrated magnet candidate, $KV_3Sb_5$, Sci. Adv. **6**, abb6003 (2020).

[38] F. H. Yu, T. Wu, Z. Y. Wang, B. Lei, W. Z. Zhuo, J. J. Ying, and X. H. Chen, Concurrence of anomalous Hall effect and charge density wave in a superconducting topological kagome metal, Phys. Rev. B **104**, L041103 (2021).

[39] H. Li, H. Zhao, B. R. Ortiz, T. Park, M. Ye, L. Balents, Z. Wang, S. D. Wilson, and I. Zeljkovic, Rotation symmetry breaking in the normal state of a kagome superconductor $KV_3Sb_5$, Nat. Phys. **18**, 265 (2022).

[40] Y. Xiang, Q. Li, Y. Li, W. Xie, H. Yang, Z. Wang, Y. Yao, and H.-H. Wen, Twofold symmetry of c-axis resistivity in topological kagome superconductor $CsV_3Sb_5$ with in-plane rotating magnetic field, Nat. Commun. **12**, 6727 (2021).

[41] H. Tan, Y. Liu, Z. Wang, and B. Yan, Charge Density Waves and Electronic Properties of Superconducting Kagome Metals, Phys. Rev. Lett. **127**, 046401 (2021).

[42] M. H. Christensen, T. Birol, B. M. Andersen, and R. M. Fernandes, Theory of the charge-density wave in $AV_3Sb_5$ kagome metals, Phys. Rev. B **104**, 214513 (2021).

[43] X. Feng, K. Jiang, Z. Wang, and J. Hu, Chiral flux phase in the Kagome superconductor $AV_3Sb_5$, Sci. Bull. **66**, 1384 (2021).

[44] M. M. Denner, R. Thomale, and T. Neupert, Analysis of Charge Order in the Kagome Metal $AV_3Sb_5$ ($A = $ K, Rb, Cs), Phys. Rev. Lett. **127**, 217601 (2021); **128**, 099901(E) (2022).

[45] Y.-P. Lin and R. M. Nandkishore, Complex charge density waves at Van Hove singularity on hexagonal lattices: Haldane-model phase diagram and potential realization in kagome metals $AV_3Sb_5$, Phys. Rev. B **104**, 045122 (2021).

[46] T. Park, M. Ye, and L. Balents, Electronic instabilities of kagomé metals: Saddle points and Landau theory, Phys. Rev. B **104**, 035142 (2021).

[47] H. X. Li, T. T. Zhang, Y.-Y. Pai, C. Marvinney, A. Said, T. Yilmaz, Q. Yin, C. Gong, Z. Tu, E. Vescovo, R. G. Moore, S. Murakami, H. C. Lei, H. N. Lee, B. Lawrie, and H. Miao, Observation of Unconventional Charge Density Wave without Acoustic Phonon Anomaly in Kagome Superconductors $AV_3Sb_5$ (A = Rb, Cs), Phys. Rev. X **11**, 031050 (2021).

[48] Z. Liang, X. Hou, F. Zhang, W. Ma, P. Wu, Z. Zhang, F. Yu, J.-J. Ying, K. Jiang, L. Shan, Z. Wang, and X.-H. Chen, Three-Dimensional Charge Density Wave and Robust Zero-Bias Conductance Peak inside the Superconducting Vortex Core of a Kagome Superconductor $CsV_3Sb_5$, Phys. Rev. X **11**, 031026 (2021).

[49] B. R. Ortiz, S. M. L. Teicher, L. Kautzsch, P. M. Sarte, J. P. C. Ruff, R. Seshadri, and S. D. Wilson, Fermi Surface Mapping and the Nature of Charge Density Wave Order in the Kagome Superconductor $CsV_3Sb_5$, Phys. Rev. X **11**, 041030 (2021).

[50] Q. Stahl, D. Chen, T. Ritschel, C. Shekhar, C. Felser, and J. Geck, Temperature-driven reorganization of electronic order in $CsV_3Sb_5$, Phys. Rev. B **105**, 195136 (2022).

[51] J. Luo, Z. Zhao, Y. Z. Zhou, J. Yang, A. F. Fang, H. T. Yang, H. J. Gao, R. Zhou, and G.-Q. Zheng, Star-of-David pattern charge density wave with additional modulation in the kagome superconductor $CsV_3Sb_5$ revealed by $^{51}$V-NMR and $^{121/123}$Sb-NQR, npj Quantum Mater. **7**, 30 (2022).

[52] See Supplemental Material at http://link.aps.org/supplemental/10.1103/PhysRevB.106.L241106 for methods, DFT calculated electronic structure of $CsV_3Sb_5$ in and CDW order, double-band splittings in $RbV_3Sb_5$, experimentally determined energy scales of the double-band splittings, and other supporting information.

[53] Y. Luo, S. Peng, S. M. L. Teicher, L. Huai, Y. Hu, Y. Han, B. R. Ortiz, Z. Liang, Z. Wei, J. Shen, Z. Ou, B. Wang, Y. Miao, M. Guo, M. Hashimoto, D. Lu, Z. Qiao, Z. Wang, S. D. Wilson, X. Chen, and J.-F. He, Electronic states dressed by an out-of-plane supermodulation in the quasi-two-dimensional kagome superconductor, $CsV_3Sb_5$, Phys. Rev. B **105**, L241111 (2022).

[54] G. Kresse and J. Hafner, Ab initio molecular dynamics for liquid metals, Phys. Rev. B **47**, 558 (1993).

[55] G. Kresse and J. Furthmüller, Efficiency of ab-initio total energy calculations for metals and semiconductors using a plane-wave basis set, Comput. Mater. Sci. **6**, 15 (1996).

[56] G. Kresse and J. Furthmüller, Efficient iterative schemes for ab initio total-energy calculations using a plane-wave basis set, Phys. Rev. B **54**, 11169 (1996).

[57] J. P. Perdew, K. Burke, and M. Ernzerhof, Generalized Gradient Approximation Made Simple, Phys. Rev. Lett. **77**, 3865 (1996).

[58] H. J. Monkhorst and J. D. Pack, Special points for Brillouin-zone integrations, Phys. Rev. B **13**, 5188 (1976).

[59] S. Grimmea, J. Antony, S. Ehrlich, and H. Krieg, A consistent and accurate ab initio parametrization of density functional dispersion correction (DFT-D) for the 94 elements H-Pu, J. Chem. Phys. **132**, 154104 (2010).

[60] V. Popescu and A. Zunger, Extracting $E$ versus $k$ effective band structure from supercell calculations on alloys and impurities, Phys. Rev. B **85**, 085201 (2012).

[61] P. V. C. Medeiros, Sven Stafström, and Jonas Björk, Effects of extrinsic and intrinsic perturbations on the electronic structure of graphene: Retaining an effective primitive cell band structure by band unfolding, Phys. Rev. B **89**, 041407(R) (2014).

[62] A. Damascelli, Z. Hussain, and Z.-X. Shen, Angle-resolved photoemission studies of the cuprate superconductors, Rev. Mod. Phys. **75**, 473 (2003).

[63] K. Nakayama, Y. Li, T. Kato, M. Liu, Z. Wang, T. Takahashi, Y. Yao, and T. Sato, Multiple energy scales and anisotropic energy gap in the charge-density-wave phase of the kagome superconductor $CsV_3Sb_5$, Phys. Rev. B **104**, L161112 (2021).

[64] Y. Cai, Y. Wang, Z. Hao, Y. Liu, X.-M. Ma, Z. Shen, Z. Jiang, Y. Yang, W. Liu, Q. Jiang, Z. Liu, M. Ye, D. Shen, Z. Sun, J. Chen, L. Wang, C. Liu, J. Lin, J. Wang, B. Huang, J.-W. Mei, and C. Chen, Emergence of Quantum Confinement in Topological Kagome Superconductor $CsV_3Sb_5$ family, arXiv:2109.12778.

[65] M. Kang, S. Fang, J. Yoo, B. R. Ortiz, Y. Oey, S. H. Ryu, J. Kim, C. Jozwiak, A. Bostwick, E. Rotenberg, E. Kaxiras, J. Checkelsky, S. D. Wilson, J.-H. Park, and R. Comin, Microscopic structure of three-dimensional charge order in kagome superconductor AV3Sb5 and its tunability, arXiv:2203.05055.

[66] Y. Xie, Yongkai Li, P. Bourges, A. Ivanov, Zijin Ye, M. Z. Hasan J.-X.Yin, A. Luo, Y. Yao, Z. Wang, G. Xu, and P. Dai, Electron-phonon coupling in the charge density wave state of $CsV_3Sb_5$, Phys. Rev. B **105**, L140501 (2022).